Dual Targeting of Endothelial Cells and Pericytes in Antivascular Therapy for Ovarian Carcinoma

Chunhua Lu,[1] Aparna A. Kamat,[1] Yvonne G. Lin,[1] William M. Merritt,[1] Charles N. Landen,[1] Tae Jin Kim,[1,3] Whitney Spannuth,[1] Thiru Arumugam,[2] Liz Y. Han,[1] Nicholas B. Jennings,[1] Craig Logsdon,[2] Robert B. Jaffe,[4] Robert L. Coleman,[1] and Anil K. Sood[1,2]

Abstract

Purpose: Pericytes are known to provide a survival advantage for endothelial cells. We hypothesize that strategies aimed at dual targeting of tumor-associated endothelial cells and pericytes will be highly efficacious.

Experimental Design: Paclitaxel-sensitive (HeyA8 and SKOV3ip1) or paclitaxel-resistant (HeyA8-MDR) orthotopic tumors in mice were examined for therapeutic efficacy by targeting the endothelial cells (using a vascular endothelial growth factor receptor inhibitor, AEE788) and pericytes (using STI571) alone or in combination. Additional therapy and survival studies in combination with paclitaxel were also done. Following therapy, tumors were examined for endothelial cell apoptosis, pericyte coverage, microvessel density, and proliferation.

Results: AEE788 inhibited tumor growth by 45% and 59% in the HeyA8 and SKOV3ip1 models, respectively, whereas STI571 alone was not effective. AEE788 plus STI571 resulted in 69% to 84% inhibition of tumor growth in both models. Moreover, combination of these agents with paclitaxel was even more effective, resulting in up to 98% inhibition of tumor growth. The triple combination was even effective in the HeyA8-MDR model. Remarkably, this triple combination also resulted in improved survival compared with all other groups ($P < 0.001$) and caused regression of formed tumors. Pericyte coverage was significantly decreased in the STI571 treatment groups, and microvessel density was significantly reduced in the AEE788 treatment groups. AEE788 induced endothelial cell apoptosis, which was further enhanced by the addition of STI571.

Conclusions: Strategies targeting both endothelial cells and pericytes are highly effective for *in vivo* treatment of ovarian carcinoma. This antiangiogenic effect may be partially due to decreased pericyte coverage, thus increasing the sensitivity of tumor vasculature to therapy. These encouraging data support the development of clinical trials based on this strategy.

Ovarian cancer remains the most common cause of death from a gynecologic malignancy. Typical treatment for women with ovarian cancer is surgical tumor cytoreduction followed by platinum and paclitaxel chemotherapy. The majority of patients respond to initial therapy, but 70% will develop recurrence and succumb to disease. Therefore, novel therapeutic strategies are urgently needed to improve the outcome of women with ovarian cancer.

The progressive growth of primary tumor and metastases is dependent on angiogenesis. Inhibition of tumor angiogenesis may provide an efficient strategy to block tumor growth because endothelial cells are genetically stable and, therefore, less likely to accumulate mutations that would allow them to develop drug resistance (1). Antiangiogenic strategies have largely focused on targeting endothelial cells. For example, vascular endothelial growth factor (VEGF) is considered to play a key role in angiogenesis and VEGF inhibitors, such as bevacizumab, are showing promise in clinical trials (2). Other blockers of VEGF/VEGF receptor (VEGFR) signaling, including PTK787 (blocks VEGFR phosphorylation) or VEGF-Trap, have potent activity in inhibiting malignant ascites and tumor growth in preclinical mouse models of ovarian carcinoma (3–6). However, VEGF targeting alone does not seem to be sufficient for regression of most bulky tumors. Although anti-VEGF therapy has resulted in improved patient survival in several tumor types (7), further improvements in cure rates may require consideration of additional targets. One such target may

be pericytes, which are mesenchymal cells that wrap around the vessel tube and are required for normal microvascular stability and function (8). Pericytes are associated with capillaries and postcapillary venules and provide structural support to endothelial cells. Pericytes covering vessels may limit the global effectiveness of antiangiogenic therapy by providing survival signals for endothelial cells (8). Therefore, we hypothesize that dual targeting of endothelial cells and pericytes would be more efficacious than targeting either cell type alone.

The platelet-derived growth factor (PDGF) ligand/receptor system (9–11) is one of the major signaling pathways for regulating pericyte homeostasis. In the current study, using an orthotopic murine model of advanced ovarian carcinoma, we examined the efficacy and mechanisms of dual targeting of endothelial cells with AEE788 (VEGFR inhibitor) and pericytes with STI571 [PDGF receptor (PDGFR) inhibitor] on ovarian cancer growth.

Materials and Methods

Cell lines and culture conditions. For these studies, we used the highly metastatic human ovarian cancer cell lines HeyA8, SKOV3ip1, and HeyA8-MDR as described previously (12, 13). Cells were grown as monolayer cultures in RPMI 1640 cell culture medium supplemented with 15% fetal bovine serum and 0.5% gentamicin. HeyA8-MDR cells were grown in the same medium supplemented with 500 ng/mL paclitaxel. Adherent monolayers were maintained on plastic and incubated at 37°C in a mixture of 5% CO_2 and 95% air. The tumor cells were free of *Mycoplasma* and pathogenic murine viruses (assayed by M.A. Bioproducts). The cultures were maintained for no longer than 12 weeks after recovery from frozen stock. The HeyA8-luciferase–transfected cell line (HeyA8-Luc) was established using a lentivirus system. The luciferase reporter was cut and removed from the pGL Vector (Promega) and cloned into the lentiviral vector FG9 with cytomegalovirus/long terminal repeat and UBiC promoter. The lentiviral vector was cotransfected with packaging vectors, and the lentivirus was produced in human embryonic 293T cells by the calcium transfection method. Lentivirus was titrated and HeyA8 cells were infected with lentivirus along with polybrene (4 μg/mL). After stable transfection of the luciferase reporter, activity was measured by adding D-luciferin (150 μg/mL), and luciferase activity was quantified by using the IVIS bioluminescence system (Xenogen Co.).

Animals. Female athymic nude mice (NCr-*nu*) were purchased from the Animal Production Area of the National Cancer Institute-Frederick Cancer Research and Development Center. The mice were housed under specific pathogen-free conditions in facilities approved by the American Association for Accreditation of Laboratory Animal Care and in agreement with current regulations and standards of the U.S. Department of Health and Human Services, the U.S. Department of Agriculture, and the NIH. Mice were used in these experiments according to institutional guidelines when they were 8 to 12 weeks old.

Drugs and reagents. AEE788 and STI571 were generously provided by Novartis Pharma AG. AEE788 is an orally active, dual tyrosine kinase inhibitor of VEGFR2 and EGFR. STI571 (imatinib mesylate, Gleevec), a derivative of 2-phenylaminopyrimidine, is an orally active highly selective tyrosine kinase inhibitor of PDGFR as well as a potent tyrosine kinase inhibitor of c-Kit. For *in vivo* oral administration, AEE788 was dissolved in *N*-methylpyrrolidone and polyethylene glycol 300 (1:9, v/v); STI571 was dissolved in distilled water. The AEE788 and STI571 solutions were prepared immediately before use. Paclitaxel (Bristol-Myers Squibb Co.) was diluted in PBS at 600 μg/mL before administration.

Orthotopic implantation of tumor cells and tumor collection procedures. To produce tumors in nude mice, subconfluent cultures of HeyA8, HeyA8-MDR, and SKOV3ip1 cells were lifted with trypsin, mixed with medium containing 10% fetal bovine serum, centrifuged at 1,000 rpm for 7 min, washed in serum-free medium, and resuspended in HBSS. Only single-cell suspensions with >95% viability, as determined by trypan blue exclusion, were used for the *in vivo* injections. Cells were then injected i.p. into female athymic mice at a concentration of $2.5 \times 10^5/0.2$ mL for HeyA8 cells and $1 \times 10^6/0.2$ mL for HeyA8-MDR and SKOV3ip1 cells. Mice were sacrificed 28 to 42 days after tumor cell injection, at which time body weight was recorded. Tumors in the peritoneal cavity were excised and weighed. For immunohistochemical staining and H&E staining procedures, tumors were fixed in formalin and embedded in paraffin. For immunofluorescence staining, terminal deoxynucleotidyl transferase–mediated dUTP nick end labeling (TUNEL), and immunohistochemistry requiring frozen tissue, tumors were embedded in OCT compound (Miles, Inc.), frozen rapidly in liquid nitrogen, and stored at -80°C.

Treatment and data collection. For therapy experiments, HeyA8, SKOV3ip1, and HeyA8-MDR cells were injected i.p., and 7 days later, mice were randomized into six groups (*n* = 10/group) and the following treatments were initiated: (*a*) vehicle control (water orally daily plus PBS i.p. weekly), (*b*) AEE788 (50 mg/kg orally thrice weekly), (*c*) STI571 (50 mg/kg orally daily), (*d*) paclitaxel (6 mg/kg i.p. weekly), (*e*) AEE788 plus STI571, and (*f*) AEE788 plus STI571 plus paclitaxel (doses in combination are the same as individual treatment groups). The doses used in these experiments were identified as optimal biological doses previously (14). Following 3 to 5 weeks of therapy, mice were sacrificed when animals in the control group became moribund. Body weights were recorded, and tumors were weighed and collected.

For the survival experiments, mice were injected i.p. with HeyA8 cells (2.5×10^5 per mouse). In the small-volume disease model, treatment was started 7 days after tumor cell injection and continued until near death or moribund. For the large tumor model, treatment was started 17 days after tumor cell injection. The mice were randomized into six groups (*n* = 10/group) and received therapy according to the doses described above. Mice were sacrificed when moribund.

In vivo bioluminescence imaging. For regression experiments, mice were injected i.p. with the HeyA8-Luc cells at 2.5×10^5 per mouse. Bioluminescence imaging was conducted on a cryogenically cooled IVIS 100 imaging system coupled to a data acquisition computer running Living Image software (Xenogen). Before imaging, animals were anesthetized in an acrylic chamber with 1.5% isoflurane/air mixture and injected i.p. with 15 mg/mL of luciferin potassium salt in PBS at a dose of 150 mg/kg body weight. A digital gray-scale animal image was acquired followed by acquisition and overlay of a pseudocolor image representing the spatial distribution of detected photon emerging from active luciferase within the animal. Signal intensity was quantified as the sum of all detected photons within the region of interest per second. After 17 days, based on bioluminescence imaging data, mice were randomized into three groups and treated as follows: (*a*) vehicle control (water orally daily plus PBS i.p. weekly), (*b*) AEE788 plus paclitaxel, or (*c*) AEE788 plus STI571 plus paclitaxel (at doses listed above). For longitudinal assessment, bioluminescence imaging was conducted at 17, 23, 25, 27, and 31 days after tumor cell injection. At the end of the experiment, animals were sacrificed and necropsy was done to assess tumor weight and number of nodules.

Immunofluorescence double staining for CD31 and desmin. Sections were fixed in cold acetone for 10 min, blocked with protein blocker for 20 min at room temperature, incubated with CD31 antibody (1:400; BD PharMingen) overnight at 4°C followed by incubation with Alexa Fluor 594–conjugated anti-rat antibody (1:1,000; Invitrogen) for 1 h at room temperature. After washing with PBS, samples were incubated with desmin antibody (1:400; DakoCytomation) for 1 h and followed by incubation with Alexa Fluor 488–conjugated anti-rabbit antibody (1:1,200; Invitrogen) for 1 h at room temperature. Samples were counterstained with Hoechst for 5 min and mounted.

Immunofluorescence staining for PDGFR and double staining for phosphorylated PDGFR and desmin. Frozen sections were fixed and processed as described above. For PDGFR staining, samples were incubated with PDGFR antibody (1:100; Santa Cruz Biotechnology) overnight at 4°C followed by incubation with Alexa Fluor 488–conjugated anti-rat antibody (1:1,000; Invitrogen) for 1 h at room temperature. For double staining of phosphorylated PDGFR and desmin, the samples were first incubated with phosphorylated PDGFR antibody (1:100; Santa Cruz Biotechnology) overnight followed by Alexa Fluor 594–conjugated anti-goat antibody (1:1,000; Invitrogen) for 1 h. After washing with PBS, samples were incubated with desmin antibody (1:400) for 1 h followed by incubation with Alexa Fluor 488–conjugated anti-rabbit antibody (1:1,200) for 1 h at room temperature. Samples were counterstained with Hoechst for 5 min and mounted.

Immunofluorescence staining for CD31 and TUNEL. Frozen sections were used as described previously (12, 15). Briefly, immunofluorescence for CD31 was assessed using Alexa Fluor 594–conjugated secondary antibody as described above. Samples were again blocked briefly in a blocking solution and then analyzed for apoptotic cells using a TUNEL kit (Promega). Samples were fixed and incubated with an equilibration buffer followed by a reaction buffer containing nucleotide mix and terminal deoxynucleotidyl transferase enzyme. Finally, samples were counterstained with Hoechst and mounted. Endothelial cells were identified by red fluorescence, and DNA fragmentation was detected by localized green fluorescence within the nucleus of apoptotic cells. An endothelial cell undergoing apoptosis was represented by yellow fluorescence. The quantification of apoptotic endothelial cells was calculated by the ratio of apoptotic endothelial cells to the total number of endothelial cells in 10 random fields at ×200 magnification.

Immunohistochemical staining for proliferating cell nuclear antigen and CD31. Paraffin-embedded tissues were used for immunohistochemical staining of proliferating cell nuclear antigen (PCNA). Immunohistochemical procedures were done as described previously (12, 13). Control samples were exposed to a secondary antibody alone and showed no evidence of nonspecific staining.

Quantification of microvessel density, PCNA, and CD31/TUNEL-positive endothelial cells and pericyte coverage. For the purpose of quantification, five samples from each group were examined. To quantify microvessel density (MVD) for each sample, the microvessels within five randomly selected 0.159-mm^2 fields at ×100 were counted. A single microvessel was defined as a discrete cluster or single cell stained positive for CD31 (CD31$^+$). The presence of a lumen was required for scoring as a microvessel. To quantify PCNA expression, the percentage of positive cells was determined in five random 0.159-mm^2 fields at ×100 magnification. To quantify apoptotic endothelial cells, the number of CD31/TUNEL double-positive cells was counted in five random 0.011-mm^2 fields at ×200 magnification. For pericyte coverage, the percentage of vessels with at least 50% coverage of associated desmin-positive cells was determined in five random 0.159-mm^2 fields at ×200 magnification for each tumor.

Statistical analysis. All measurements are depicted as the average ± SE of the mean. Continuous variables were compared with the Student's *t* test or ANOVA if normally distributed and the Mann-Whitney rank sum test if distributions were nonparametric using Statistical Package for the Social Sciences (SPSS, Inc.). Kaplan-Meier survival plots were generated and comparisons between survival curves were made using the log-rank statistic. A *P* value of <0.05 was considered statistically significant.

Results

Effect of endothelial and pericyte targeting on ovarian cancer growth. To determine the efficacy of combinatorial approaches for ovarian cancer treatment, we used the HeyA8 and SKOV3ip1 models because they represent the growth patterns seen in women with metastatic ovarian cancer. For therapy experiments, 7 days after tumor cell injection, mice were randomized into the following six groups: (*a*) vehicle control, (*b*) AEE788 alone, (*c*) STI571, (*d*) paclitaxel, (*e*) AEE788 plus STI571, and (*f*) AEE788 plus STI571 plus paclitaxel. In the HeyA8 model, AEE788 alone and in combination with STI571 led to a 45% and 59% reduction in tumor growth compared with controls, respectively (Fig. 1A). STI571 alone had no effect on tumor growth. Similarly, in the SKOV3ip1 model, AEE788 alone and in combination with STI571 was effective in inhibiting tumor growth, whereas STI571 alone had no effect on tumor growth. The combination of these three agents (AEE788, STI571, and paclitaxel) resulted in 94% and 98% inhibition of tumor growth in the HeyA8 and SKOV3ip1 models, respectively, compared with controls. There were no differences in mouse weights between the six treatment groups, suggesting that eating and drinking habits were not affected.

A common clinical problem in the management of patients with ovarian cancer is the development of chemotherapy resistance. To address potential efficacy of dual endothelial and pericyte targeting in a chemotherapy-resistant model, we used the taxane-resistant HeyA8-MDR model. As expected, paclitaxel alone had no effect (Fig. 1A). AEE788 alone resulted in a 46% reduction of tumor growth, and AEE788 plus STI571 led to a 65% reduction of tumor growth over controls. Remarkably, the combination of AEE788, STI571, and paclitaxel was significantly superior to other groups, resulting in 88% reduction in tumor growth.

Based on the promising results with regard to inhibition of tumor growth, we next examined the effects of dual endothelial and pericyte-targeted therapy on survival. Therapy was initiated 7 days after injection of tumor cells and continued until individual animals became moribund. Because the greatest benefit in the therapy experiments was derived when chemotherapy was added to the biological therapy, for this experiment, we combined paclitaxel with each individual agent. Treatment with paclitaxel alone or in combination with AEE788 or STI571 resulted in a modest improvement in survival (each *P* < 0.05; Fig. 1B). Remarkably, the greatest improvement in survival was noted with the triple combination (*P* < 0.001; Fig. 1B).

Effect of dual endothelial and pericyte targeting on established ovarian tumor regression. Although the models described above recapitulate disease patterns of patients with small-volume disease, many patients with relapsed ovarian cancer have larger tumor burden. Therefore, we also examined the potential of dual endothelial and pericyte-targeted therapy to cause regression of larger tumors. Because it is difficult to take sequential measurements of ovarian tumors in an orthotopic setting, we used an *in vivo* bioluminescence imaging system for longitudinal assessments. The HeyA8-Luc cells were inoculated into the peritoneal cavity of nude mice, and baseline imaging was done on day 10. Following initiation of therapy on day 17, *in vivo* bioluminescence imaging was done at 2- to 6-day intervals and the experiment was terminated when controls became moribund. Based on the survival data noted above and our previous data (14) about the efficacy of AEE788 in combination with paclitaxel, we used this combination for comparison. Interestingly, the triple treatment resulted in regression of formed tumors by up to 75% (based on photon
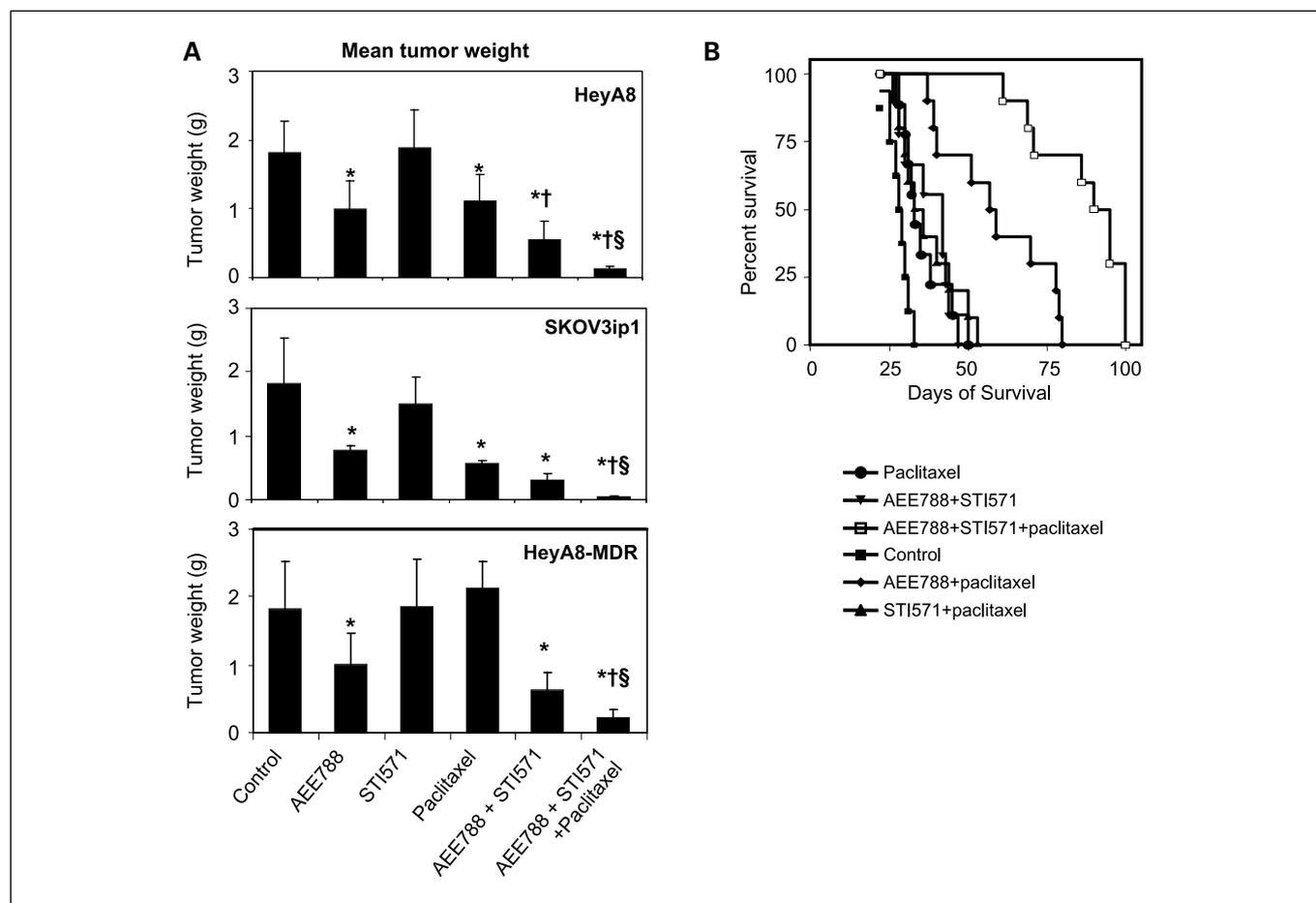
Fig. 1. Effect of dual endothelial and pericyte targeting on human ovarian cancer growth. *A,* mice were injected with HeyA8, SKOV3ip1, or HeyA8-MDR human ovarian cancer cells. Seven days later, mice were randomized (*n* = 10) to receive the following regimens: (*a*) vehicle control, (*b*) AEE788 alone, (*c*) STI571 alone, (*d*) paclitaxel alone, (*e*) AEE788 plus STI571, and (*f*) AEE788 plus STI571 in combination with paclitaxel. Mice were sacrificed when control mice were moribund (4-6 weeks after tumor cell injection). Columns, mean tumor weights; bars, SE. *, $P < 0.05$, compared with vehicle controls; †, $P < 0.05$, compared with AEE788; §, $P < 0.05$, compared with AEE788 plus STI571 group. *B,* the effect of antivascular therapy on survival in the HeyA8 model with initiation of therapy at 7 days following tumor cell injection was determined using Kaplan-Meier estimates.

counts) after 10 days of treatment (Fig. 2A). Although tumors grew slower with AEE788 plus paclitaxel, no apparent tumor regression was noted with this combination.

We also determined the effect of dual endothelial and pericyte targeting strategies on survival in the presence of larger tumors. For these experiments, therapy was started at 17 days after tumor cell inoculation. Even with larger tumors, the triple combination of AEE788, STI571, and paclitaxel had the greatest effect on prolonging survival compared with all other treatment groups ($P < 0.001$; Fig. 2B).

Effect of dual endothelial and pericyte targeting on MVD and vessel maturation. To examine potential mechanisms underlying the efficacy of the approaches presented above, we first assessed the extent of MVD (using CD31 staining) in tumor tissue following treatments. As shown in Fig. 3A, MVD was significantly reduced in the AEE788-only group ($P < 0.05$ versus control), AEE788 plus STI571 group ($P < 0.05$ versus AEE788-only group), and the triple combination group ($P < 0.05$ versus all groups). STI571 alone did not affect MVD.

STI571 was effective in blocking PDGFR phosphorylation in pericytes without affecting total PDGFR levels (Supplementary Fig. S1). We next examined the extent of pericyte coverage of tumor blood vessels using double immunofluorescence staining for desmin (pericyte marker) and CD31. As shown in Fig. 3B, 68% of the blood vessels in the HeyA8 tumors had pericyte coverage. Interestingly, treatment with AEE788 monotherapy resulted in increased pericyte coverage to 91% ($P < 0.05$). In contrast, treatment with STI571 significantly decreased pericyte coverage to 39%. The proportion of blood vessels with pericyte coverage was significantly decreased in the AEE788 plus STI571 group and in the triple combination group ($P < 0.05$; Fig. 3B). Treatment with paclitaxel alone did not alter vessel maturation.

Effect of dual endothelial and pericyte targeting on endothelial cell apoptosis in tumor tissue. It has been hypothesized that pericytes protect endothelial cells from the apoptotic effects of antiangiogenesis therapy (16, 17). Therefore, we used dual immunofluorescence (CD31/TUNEL) to evaluate for apoptosis of tumor-associated endothelial cells in the HeyA8 tumors following treatment with AEE788, STI571, and paclitaxel alone or in combination. As shown in Fig. 4A, minimal endothelial cell apoptosis was apparent in either the control or single-agent STI571 treatment groups. The greatest increase in endothelial cell apoptosis was noted in the triple combination group ($P < 0.01$; Fig. 4A). These data suggest that the triple combination

therapy can induce tumor regression, at least in part, by reducing pericyte coverage and promoting endothelial cell apoptosis.

Effect of dual endothelial and pericyte targeting on tumor cell proliferation. To examine the effects of therapy on proliferation, we did immunostaining for PCNA. Proliferation was not significantly altered in paclitaxel-only or STI571-only treatment groups (Fig. 4B). However, proliferation was significantly decreased in the AEE788 ($P < 0.05$ versus controls) and AEE788 plus STI571 ($P < 0.05$) groups. The greatest reduction in proliferation was noted in the triple combination group ($P < 0.05$ versus all groups).

Discussion

In the present study, we show that pharmacologic targeting of both endothelial cells and pericytes substantially affects *in vivo* tumor growth and regression and significantly improves survival in our orthotopic ovarian cancer mouse model, particularly in combination with taxane chemotherapy. We have shown the effect of this effect in both small- and large-volume tumors as well as in taxane-resistant tumors. Targeting pericytes in these experiments with STI571 led to enhanced endothelial cell apoptosis and decreased tumor proliferation when combined with AEE788 and when added to combination paclitaxel and AEE788. Collectively, we show that pericyte targeting is feasible and important to a therapeutic strategy addressing newly formed and established tumor-associated vasculature.

VEGF plays a critical role in developmental, physiologic, and pathologic neovascularization and mediates endothelial cell proliferation and survival (18–20). However, VEGF targeting alone does not seem sufficient to cause regression of most bulky tumors. One explanation for this observation may be
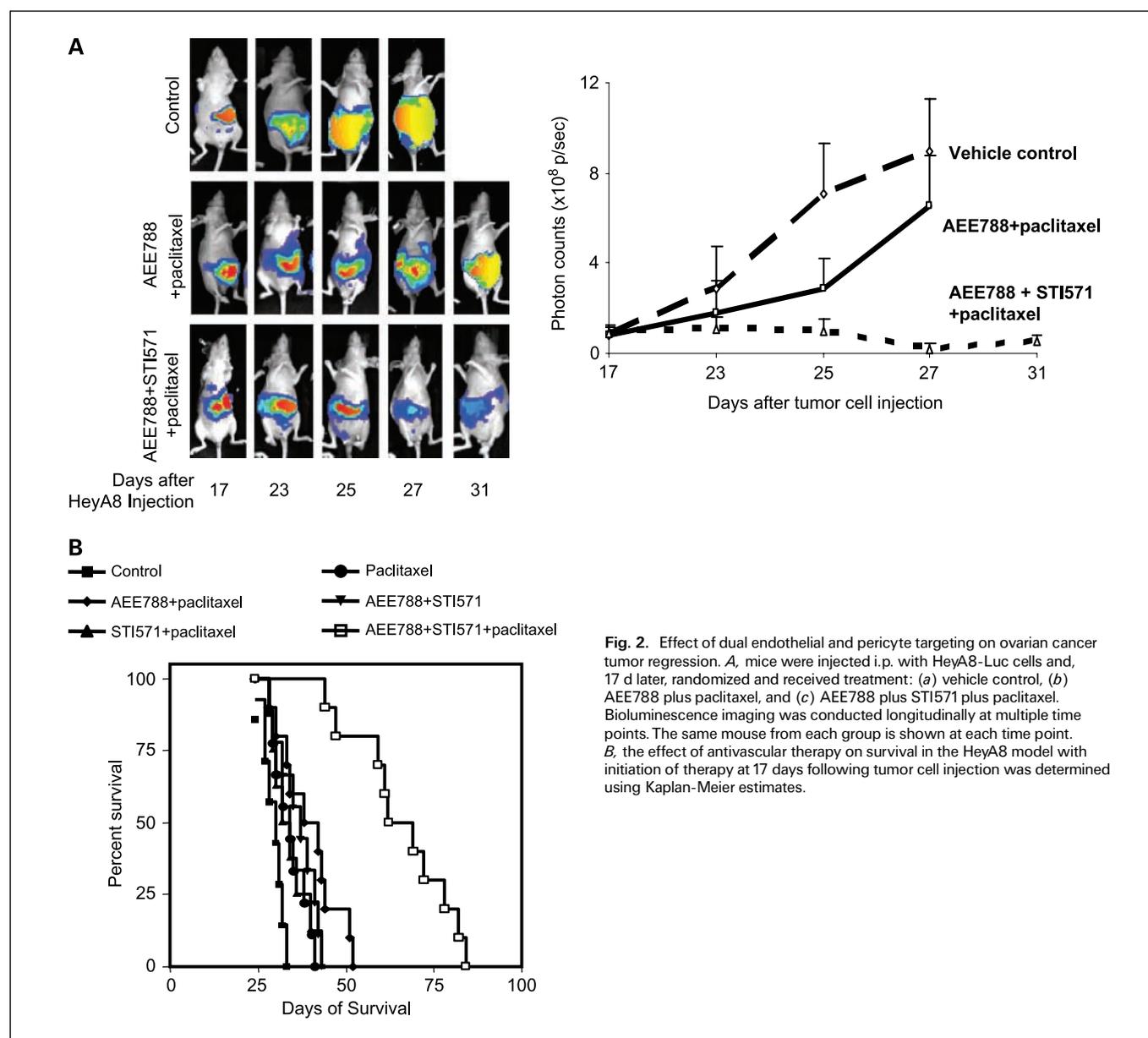

Fig. 2. Effect of dual endothelial and pericyte targeting on ovarian cancer tumor regression. *A,* mice were injected i.p. with HeyA8-Luc cells and, 17 d later, randomized and received treatment: (*a*) vehicle control, (*b*) AEE788 plus paclitaxel, and (*c*) AEE788 plus STI571 plus paclitaxel. Bioluminescence imaging was conducted longitudinally at multiple time points. The same mouse from each group is shown at each time point. *B,* the effect of antivascular therapy on survival in the HeyA8 model with initiation of therapy at 17 days following tumor cell injection was determined using Kaplan-Meier estimates.
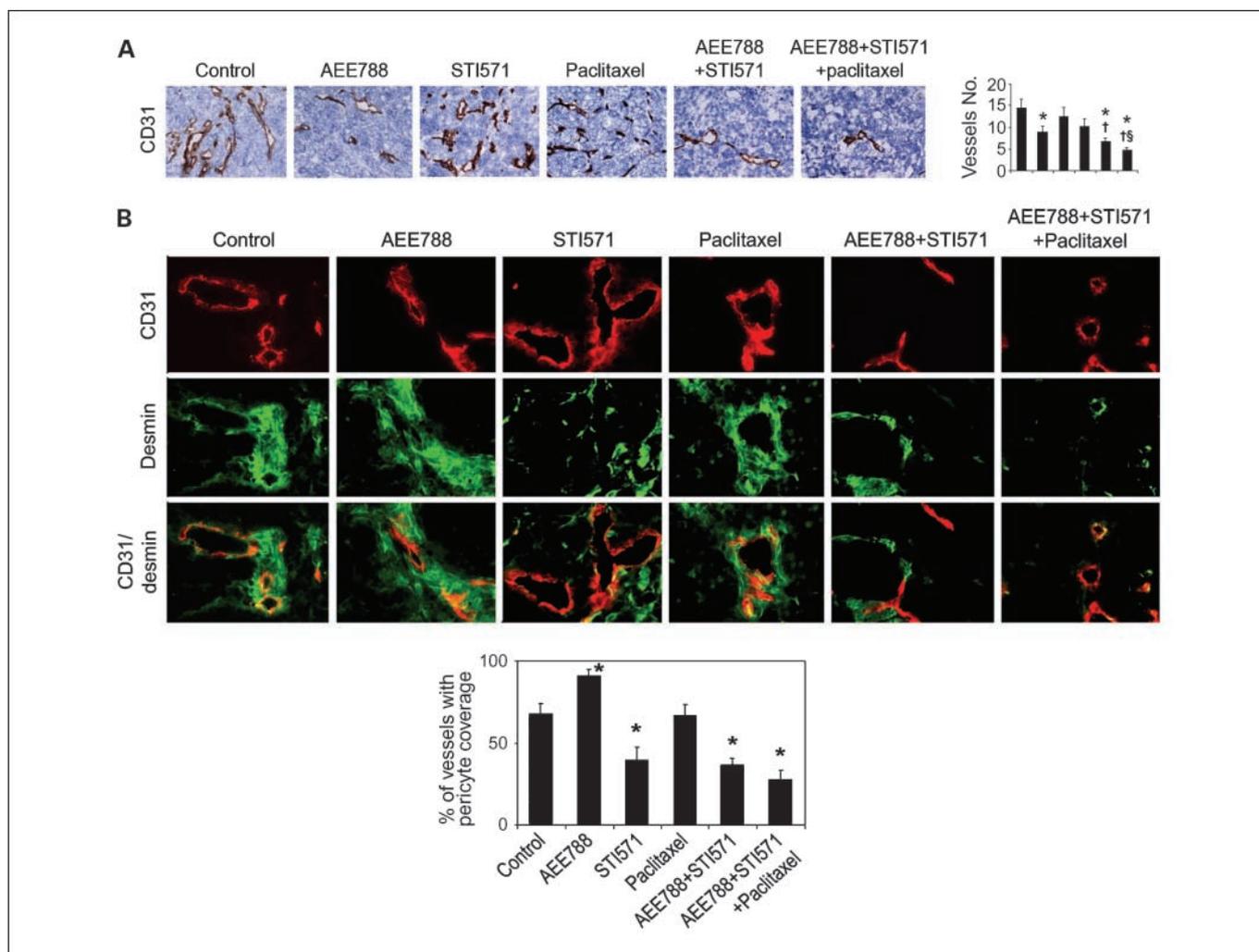
Fig. 3. Effect of dual endothelial and pericyte targeting on tumor vasculature. *A,* tumor sections were stained with CD31 using immunohistochemical staining to reveal MVD. Microvessels were counted and graphed. *, $P < 0.05$, compared with vehicle controls; †, $P < 0.05$, compared with AEE788 alone group; §, $P < 0.05$, compared with AEE788 plus STI571 group. Images were taken at original magnification of ×200. *B,* immunofluorescence double staining for CD31 (endothelial marker; *red*) and desmin (pericyte marker; *green*) was done to determine the extent of pericyte coverage. The percentage of vessels with at least 50% coverage of associated desmin-positive cells was calculated. *, $P < 0.05$, compared with vehicle controls. Images were taken at original magnification of ×400.

related to pericytes, which can provide local survival signals for endothelial cells (8). Pericytes are multibranched, elongated periendothelial cells, which are closely approximated to endothelial cells and directly communicate with them through gap junctions (21). The high density of these cells around vessels of normal tissues with substantive metabolic function highlights their attendant role in vessel structural integrity. In this capacity, reduction of pericyte density can lead to functional defects of normal vasculature. For example, loss of pericyte density is an early histopathologic finding in the development of diabetic retinopathy (22). Pericyte loss in this case is associated with thickening of the basement membrane, hyperpermeability, and microaneurysm formation, leading to microvascular occlusion. Similarly, pericytes play a crucial role in angiogenesis. Under physiologic circumstances, pericytes may respond to angiogenic stimuli, such as VEGF and guide sprouting tubes, promote endothelial stability through matrix deposition, and have macrophage-like function (23). The role of pericytes in tumor angiogenesis is less well understood but

seems to include microvascular stability and function. It has been shown by our group and others that pericytes are abundant on tumor blood vessels and, although abnormal in appearance, are intimately involved in eventual endothelial cell maturation and quiescence as well as stabilization of nascent cancer microvessels (8, 24, 25). The critical and dynamic function pericytes play in endothelial homeostasis and carcinogenesis make them a desirable subject for pharmacologic targeting.

We have previously shown that tumor-associated endothelial cells express VEGFR and EGFR and phosphorylation of these receptors is important for cell survival (14). In addition, tumor and endothelial cells produce PDGF-BB, which stimulates pericytes to produce VEGF (26). In the tumor microenvironment, this function may act locally as a survival factor for endothelial cells (26–28).[5] In addition, transforming growth
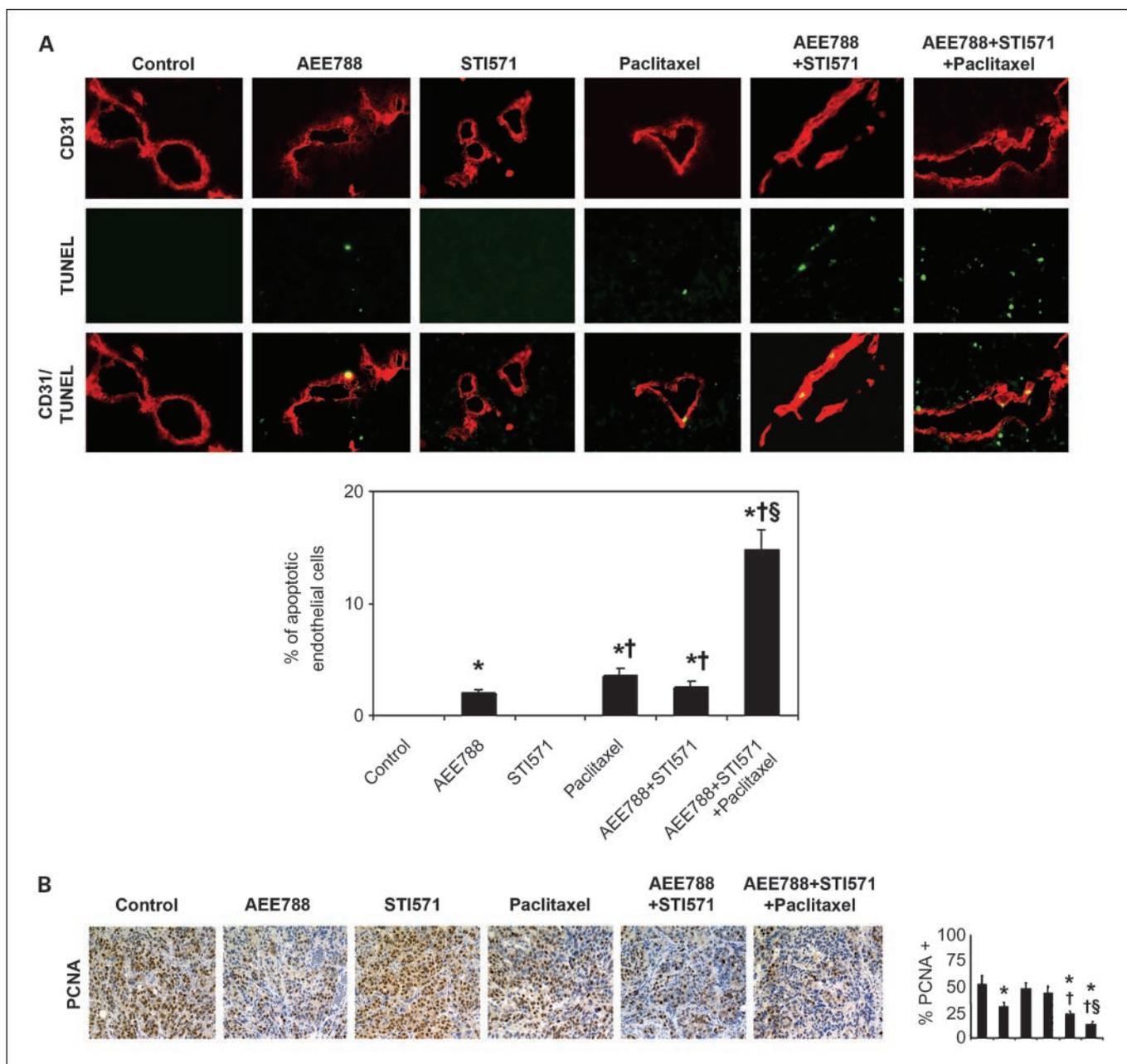
---

[5] Unpublished data.

Fig. 4. Effect of dual endothelial and pericyte targeting on endothelial cell apoptosis and tumor cell proliferation. *A,* tumor sections were stained with CD31 (*red*) and TUNEL (apoptotic marker; *green*) using double immunofluorescence staining. Colocalization of endothelial cells undergoing apoptosis shows yellow fluorescence. *, $P < 0.05$, compared with vehicle controls; †, $P < 0.05$, compared with AEE788 alone group; §, $P < 0.05$, compared with AEE788 plus STI571 group. Images were taken at original magnification of ×400. *B,* tumor sections were stained with PCNA to reveal tumor cell proliferation. PCNA-positive cells were counted and graphed. *, $P < 0.05$, compared with vehicle controls; †, $P < 0.05$, compared with AEE788 alone group; §, $P < 0.05$, compared with AEE788 plus STI571 group. Images were taken at original magnification of ×200.

factor-β1 production by pericytes may reduce the proliferation of endothelial cells through binding to Alk5, a transforming growth factor type I receptor found on pericytes (29). Although AEE788 alone and in combination with paclitaxel does not affect tumor-associated endothelial cell expression of VEGFR and EGFR, it substantially reduces receptor phosphorylation. In the present study, AEE788 reduced MVD, but the proportion of vessels with pericyte-coated vessels was increased, suggesting that pericytes may indeed protect these vessels from antiangiogenic therapy. Tumor vessels that lack pericytes seem to be

more dependent on VEGF for their survival than vessels invested by pericytes (8). Therefore, the combination of antiendothelial and antipericyte agents may have additive or synergistic activity. Results from our experiments support this hypothesis as dual endothelial (via AEE788) and pericyte (via STI571) targeting was more effective than either agent alone. The efficacy was even greater in combination with taxane chemotherapy. Remarkably, this approach was effective in both growth inhibition and tumor regression experiments. Similar results were found by Yokoi et al. (30) in an orthotopic human

pancreatic carcinoma model. Bergers et al. (25) used the RIP1-Tag2 pancreatic β-cell tumor model to test the efficacy of SU5416 (VEGFR inhibitor) and SU6668 (PDGFR inhibitor) or STI571 (PDGFR inhibitor). The combination of SU6668 or STI571 with SU5416 was most effective in reducing tumor growth, even with larger-sized tumors, where inhibition of VEGF signaling alone was insufficient (25). Similar observations have been reported by Kim et al. (31), showing that blocking EGFR phosphorylation and PDGFR together with paclitaxel significantly suppressed human prostate cancer bone metastasis.

In light of the central role pericytes seem to play in endothelial homeostasis, it is likely that tumor vessels lacking pericytes would be more dependent on VEGF for their survival than vessels invested by pericytes. Thus, if pericytes were absent or could not produce VEGF, the endothelium theoretically would become vulnerable to VEGF blockade. We showed, in this report, that inhibition of PDGFR activation by STI571 alone was insufficient to induce endothelial cell apoptosis. However, STI571 therapy significantly increased the sensitivity of dividing tumor-associated endothelial cells to the effect of AEE788 alone and in combination with paclitaxel. In this manner, receptor tyrosine kinase inhibitors with multiple targets may exert their antitumor activity in part by reducing pericyte density on the tumor vessels, thereby sensitizing them to inhibition of endothelial cell receptor tyrosine kinases. Tumor cell proliferation was similarly unaffected by PDGFR blockade alone. However, the combination of AEE788, STI571, and paclitaxel led to substantial reduction in tumor cell proliferation, suggesting significant modulation in VEGF-dependent growth signaling. The combined targeting of these agents and their availability for clinical use provide an attractive approach for therapeutic management of patients with established tumors.

A potential confounding factor in the interpretation of our results is the relative nonspecificity of the agents used. STI571 is known also to inhibit c-Kit and bcr-abl signaling. Although it is possible that these pathways may be important for tumor growth in our model, activated c-Kit is not usually present in ovarian carcinoma (32). Inhibition of PDGF signaling through more specific agents, such as PDGF-aptamer or PDGF-Trap, may be instructive in future studies. In addition, we have previously shown that AEE788 can affect phosphorylation of EGFR, which had substantive effects on *in vivo* tumor growth. Further, it is unknown whether EGFR blockade has a specific effect on pericytes. Although epidermal growth factor receptors are also present in high concentration at the cytoplasmic interdigitations between endothelial cells and pericytes and may have focal growth signaling effects, the specific effect on pericyte function in the presence of EGFR blockade is unknown (33). Nevertheless, the greatest efficacy was observed when AEE788 and STI571 were combined with paclitaxel.

In conclusion, our data show that strategies targeting both endothelial cells and pericytes are more effective than either alone for *in vivo* treatment of ovarian carcinoma, especially when combined with paclitaxel chemotherapy, even in established or drug-resistant tumors. Inhibition of VEGF and PDGF will likely be a potent antivascular strategy, inducing endothelial cell apoptosis, tumor vessel destabilization, and regression. This study provides the preclinical rationale for the development of more effective strategies for management of human ovarian cancer metastasis.

Acknowledgments

References

1. Fidler IJ. The organ microenvironment and cancer metastasis. Differentiation 2002;70:498–505.
2. Frumovitz M, Bodurka DC, Broaddus RR, et al. Lymphatic mapping and sentinel node biopsy in women with high-risk endometrial cancer. Gynecol Oncol 2007;104:100–3.
3. Byrne AT, Ross L, Holash J, et al. Vascular endothelial growth factor-trap decreases tumor burden, inhibits ascites, and causes dramatic vascular remodeling in an ovarian cancer model. Clin Cancer Res 2003;9:5721–8.
4. Hu L, Hofmann J, Holash J, et al. Vascular endothelial growth factor trap combined with paclitaxel strikingly inhibits tumor and ascites, prolonging survival in a human ovarian cancer model. Clin Cancer Res 2005;11:6966–71.
5. Mesiano S, Ferrara N, Jaffe RB. Role of vascular endothelial growth factor in ovarian cancer: inhibition of ascites formation by immunoneutralization. Am J Pathol 1998;153:1249–56.
6. Xu L, Yoneda J, Herrera C, et al. Inhibition of malignant ascites and growth of human ovarian carcinoma by oral administration of a potent inhibitor of the vascular endothelial growth factor receptor tyrosine kinases. Int J Oncol 2000;16:445–54.
7. Jain RK, Duda DG, Clark JW, et al. Lessons from phase III clinical trials on anti-VEGF therapy for cancer. Nat Clin Pract Oncol 2006;3:24–40.
8. Lu C, Sood AK. Role of pericytes in angiogenesis. Angiogenesis agents in cancer therapy. 2nd ed. The Humana Press, Inc. In press 2007.
9. Pietras K, Hanahan D. A multitargeted, metronomic, and maximum-tolerated dose "chemo-switch" regimen is antiangiogenic, producing objective responses and survival benefit in a mouse model of cancer. J Clin Oncol 2005;23:939–52.
10. Lindblom P, Gerhardt H, Liebner S, et al. Endothelial PDGF-B retention is required for proper investment of pericytes in the microvessel wall. Genes Dev 2003;17:1835–40.
11. Lindahl P, Johansson BR, Leveen P, et al. Pericyte loss and microaneurysm formation in PDGF-B-deficient mice. Science 1997;277:242–5.
12. Apte SM, Fan D, Killion JJ, et al. Targeting the platelet-derived growth factor receptor in antivascular therapy for human ovarian carcinoma. Clin Cancer Res 2004;10:897–908.
13. Thaker PH, Han LY, Kamat AA, et al. Chronic stress promotes tumor growth and angiogenesis in a mouse model of ovarian carcinoma. Nat Med 2006;12:939–44.
14. Thaker PH, Yazici S, Nilsson MB, et al. Antivascular therapy for orthotopic human ovarian carcinoma through blockade of the vascular endothelial growth factor and epidermal growth factor receptors. Clin Cancer Res 2005;11:4923–33.
15. Baker CH, Kedar D, McCarty MF, et al. Blockade of epidermal growth factor receptor signaling on tumor cells and tumor-associated endothelial cells for therapy of human carcinomas. Am J Pathol 2002;161:929–38.
16. Benjamin LE, Golijanin D, Itin A, et al. Selective ablation of immature blood vessels in established human tumors follows vascular endothelial growth factor withdrawal. J Clin Invest 1999;103:159–65.
17. Gee MS, Procopio WN, Makonnen S, et al. Tumor vessel development and maturation impose limits on the effectiveness of anti-vascular therapy. Am J Pathol 2003;162:183–93.
18. Carmeliet P, Ferreira V, Breier G, et al. Abnormal blood vessel development and lethality in embryos lacking a single VEGF allele. Nature 1996;380:435–9.
19. Carmeliet P, Moons L, Luttun A, et al. Synergism between vascular endothelial growth factor and placental growth factor contributes to angiogenesis and plasma extravasation in pathological conditions. Nat Med 2001;7:575–83.
20. Senger DR, Galli SJ, Dvorak AM, et al. Tumor cells secrete a vascular permeability factor that promotes accumulation of ascites fluid. Science 1983;219:983–5.
21. Larson DM, Carson MP, Haudenschild CC. Junctional transfer of small molecules in cultured bovine brain microvascular endothelial cells and pericytes. Microvasc Res 1987;34:184–99.
22. Engerman RL, Kern TS. Retinopathy in animal models of diabetes. Diabetes Metab Rev 1995;11:109–20.
23. Thomas WE. Brain macrophages: on the role of pericytes and perivascular cells. Brain Res Brain Res Rev 1999;31:42–57.
24. Armulik A, Abramsson A, Betsholtz C. Endothelial/pericyte interactions. Circ Res 2005;97:512–23.
25. Bergers G, Song S, Meyer-Morse N, et al. Benefits of targeting both pericytes and endothelial cells in the tumor vasculature with kinase inhibitors. J Clin Invest 2003;111:1287–95.
26. Reinmuth N, Liu W, Jung YD, et al. Induction of

VEGF in perivascular cells defines a potential paracrine mechanism for endothelial cell survival. FASEB J 2001;15:1239–41.

27. Brown EB, Campbell RB, Tsuzuki Y, et al. *In vivo* measurement of gene expression, angiogenesis and physiological function in tumors using multiphoton laser scanning microscopy. Nat Med 2001;7:864–8.

28. Fukumura D, Xavier R, Sugiura T, et al. Tumor induction of VEGF promoter activity in stromal cells. Cell 1998;94:715–25.

29. Chantrain CF, Henriet P, Jodele S, et al. Mechanisms of pericyte recruitment in tumour angiogenesis: a new role for metalloproteinases. Eur J Cancer 2006;42:310–8.

30. Yokoi K, Sasaki T, Bucana CD, et al. Simultaneous inhibition of EGFR, VEGFR, and platelet-derived growth factor receptor signaling combined with gemcitabine produces therapy of human pancreatic carcinoma and prolongs survival in an orthotopic nude mouse model. Cancer Res 2005;65:10371–80.

31. Kim SJ, Uehara H, Yazici S, et al. Simultaneous blockade of platelet-derived growth factor-receptor and epidermal growth factor-receptor signaling and systemic administration of paclitaxel as therapy for human prostate cancer metastasis in bone of nude mice. Cancer Res 2004;64:4201–8.

32. Kim SJ, Uehara H, Yazici S, et al. Targeting platelet-derived growth factor receptor on endothelial cells of multidrug-resistant prostate cancer. J Natl Cancer Inst 2006;98:783–93.

33. Wakui S. Epidermal growth factor receptor at endothelial cell and pericyte interdigitation in human granulation tissue. Microvasc Res 1992;44:255–62.

Dual Targeting of Endothelial Cells and Pericytes in Antivascular Therapy for Ovarian Carcinoma

Chunhua Lu, Aparna A. Kamat, Yvonne G. Lin, et al.

Updated version	Access the most recent version of this article at: http://clincancerres.aacrjournals.org/content/13/14/4209

Cited articles	This article cites 32 articles, 11 of which you can access for free at: http://clincancerres.aacrjournals.org/content/13/14/4209.full#ref-list-1
Citing articles	This article has been cited by 13 HighWire-hosted articles. Access the articles at: http://clincancerres.aacrjournals.org/content/13/14/4209.full#related-urls

E-mail alerts	Sign up to receive free email-alerts related to this article or journal.
Reprints and Subscriptions	To order reprints of this article or to subscribe to the journal, contact the AACR Publications Department at pubs@aacr.org.
Permissions	To request permission to re-use all or part of this article, use this link http://clincancerres.aacrjournals.org/content/13/14/4209. Click on "Request Permissions" which will take you to the Copyright Clearance Center's (CCC) Rightslink site.